Journal of Building Engineering 38 (2021) 102199

Contents lists available at ScienceDirect

Journal of Building Engineering

journal homepage: http://www.elsevier.com/locate/jobe

Recycling biosolids as cement composites in raw, pyrolyzed and ashed forms: A waste utilisation approach to support circular economy

Rajeev Roychand [a,*], Savankumar Patel [a], Pobitra Halder [a], Sazal Kundu [a], James Hampton [b], David Bergmann [b], Aravind Surapaneni [b,c], Kalpit Shah [a,c], Biplob Kumar Pramanik [a,**]

[a] School of Engineering, RMIT University, Melbourne, Victoria, 3000, Australia
[b] South East Water, Frankston, Victoria, 3199, Australia
[c] ARC Training Centre on Advance Transformation of Australia's Biosolids Resources, RMIT University, Bundoora, 3083, Australia

ARTICLE INFO

Keywords:
Biosolids
Biochar
Bioash
Cement replacement
Pyrolysis

ABSTRACT

Ongoing management of biosolids has emerged as a major economic challenge for wastewater treatment facilities around the world. To tackle this challenge, it becomes imperative for the researcher community to identify various applications for this waste material, simultaneously supporting the government's closed-loop circular economy initiative. This research investigates the use of biosolids in raw, pyrolyzed (biochar), and ashed (bioash) forms as cement replacement materials. Detailed material characterization was carried out on the raw cementitious material followed by that on the hydrated cement composites using X-ray fluorescence, X-ray diffraction, energy-dispersive X-ray spectroscopy, scanning electron microscopy, carbon, hydrogen, nitrogen, and sulfur (CHNS) analysis, Xray micro-computed tomography and compressive strength test to identify their mechanical and physicochemical properties. The results show that the addition of 10% biosolids in the blended cement composite increased its total porosity by more than 21 times and decreased its compressive strength by 80% at 28 days of curing, indicating its potential use as an air-entraining admixture for the low-density concrete. However, the addition of 10% biochar brought about a strength improvement of ~278% and a reduction in its total porosity by ~87% compared to that of the biosolids blended cement composites. Partial replacement of cement with 10% bioash (ash form) showed ~66% reduction in its total porosity and 11% reduction in the 28-day compressive-strength compared to that of the biochar blended cement composites. Overall, this study demonstrates that the different forms of biosolids (raw, biochar, and bioash) can potentially be used as cement replacement materials with varied benefits in the cement and concrete industry. The recommendation for the future work is to carry out long-term durability studies on these blended cement composites for the ready uptake of this waste material by the construction industry.

1. Introduction

Globally, it has been accepted that the make, use, and throw policy is unsustainable and negatively impact the environment, economy, and public health. Realising this concern, governments all over the world are looking for scientific solutions to recycle all forms of waste materials to develop a closed-loop circular economy, where today's waste is tomorrow's raw material. The support available from the government for various research and development activities is making it easier for the research community to develop various scientific solutions for the recycling of various forms of industrial, agricultural, and residential wastes. The construction industry is one of the major sectors that has looked at utilizing these waste materials. Flyash [1–3], slag [4–6], recycled concrete aggregates [7–11], waste tyre rubber [12–16], and waste glass [17–19] are some of the industrial waste materials that have found applications in the cement and concrete industry. Many agricultural waste materials [20,21] like rice husk ash, palm oil fuel ash, and corn cob ash have also shown great potential as cement replacement materials.

Biosolids is one of the waste materials that is actively being researched for its large volume of production, which is increasing over time because of the growing population and low utilisation rate [20,21].

* Corresponding author.
** Corresponding author.
E-mail addresses: rajeev.roychand@rmit.edu.au (R. Roychand), biplob.pramanik@rmit.edu.au (B.K. Pramanik).

https://doi.org/10.1016/j.jobe.2021.102199
Received 8 November 2020; Received in revised form 28 December 2020; Accepted 18 January 2021
Available online 21 January 2021

As per Australia and New Zealand biosolids partnership (ANZBP) commissioned survey report in 2019, Australia produced about 371,000 tonnes of dry biosolids annually, which has increased by 20% from 300,000 tonnes in 2010. Currently, the most common and major applications of biosolids are agriculture and land rehabilitation [22,23]. However, as the research advances in this field, the concerns about the transfer of pathogens [24,25] and heavy metals from biosolids into the soil are also growing [26,27]. Recently, biosolids have been recognised as a potential source of soil and groundwater contamination from per- and polyfluoroalkyl substances and micro-plastics [28], that may restrict their land application in the near future [29,30].

As an alternative, biosolids managers at wastewater treatment plants (WWTPs) have started exploring different options for biosolids management other than land applications to increase its utilisation rate. There are studies reported where biosolids have been successfully applied into brick manufacturing [31,32]. Ukwatta et al. [31] investigated the effect of incorporating biosolids obtained from a water treatment plant into fired-clay bricks. The clay used for brick manufacturing was partially replaced with 25 wt% of biosolids taken from three different stockpile locations. They observed a reduction of 28.3, 51.8, and 55.1% in the compressive strength of biosolid clay composite bricks compared to that of the control clay bricks not containing any biosolids. They noticed a corresponding increase in the total porosity and the loss on ignition of the organic content of biosolid amended clay bricks compared to that of the control samples that were instrumental in reducing their corresponding compressive strengths. Another study by Mozo-Moreno and Gómez [32] looked at replacing brick manufacturing clay with 5, 10, and 15% of biosolids content at three different kiln temperatures of 950, 1000, and 1050 °C. They observed that the compressive strength of the biosolids bricks decreased with the increase in the biosolids content indicating the negative effect of the addition of biosolids to the compressive strength of the clay-biosolids blended bricks. However, the strength of control and biosolids-clay blended bricks of all replacement levels increased with the increase in the kiln temperature. The strengths reduction in the biosolids-clay blended bricks 950 °C kiln temperature was 43.9, 54.4, 79.3% at 5, 10, 15% replacement levels, compared to that of the control bricks. However, at the kiln temperature of 1050 °C they observed a reduction in their corresponding compressive strengths by 30.1, 63, 69.2%, respectively.

There is also a growing interest among the biosolids management community that biosolids are processed onsite via pyrolysis (biochar), gasification, or incineration (bioash) methods. This allows significant reduction in its volume [33], carbon sequestration [34–36], and destruction of pathogens and emerging contaminants such as Per- and polyfluoroalkyl substances (PFAS) and micro-plastics [37–40]. Although biochar derived from various sources, such as poultry litter [41], rice husk [41,42], bagasse [42], paper mill sludge [41], wood waste [35], and agriculture waste [42] have been used as cement replacement materials, there appears to be very little, or no study carried out on the application of biochar derived from municipal waste. Akhtar and Sarmah [41] investigated the effect of replacing cement with three different types of biochars, i.e., poultry litter (PL) biochar, rice husk (RH) biochar, and pulp and paper mill sludge (PP) biochar at 0.1–1% of the total volume of concrete. They observed that the PL biochar showed a small reduction in its 7-day compressive strengths; however, the RH and PP biochars showed a considerable increase in their corresponding 7-day compressive strength results at 0.1% biochar content level, which they attributed to the early pozzolanic effect of these biochars. At 28 days of curing all types of biochars showed a reduction in their corresponding compressive strength results compared to that of the control mix, with PL biochar showing the highest reduction in its relative compressive strength. The other two biochars i.e. RH and PP showed relatively a small reduction in their corresponding compressive strength results. They also observed different trends on the effect of increasing the biochar contents with different biochar types. The PL biochar showed a significant reduction in its corresponding compressive strength at 0.25% replacement level compared to that of 0.1%, which recovered considerably at 0.5% replacement level and then somewhat stayed stable at 0.75 and 1% replacement levels at 28 days of curing. The RH biochar showed a staggered trend with the increase in its replacement level. It showed a significant reduction in its compressive strength when the replacement level increased from 0.1 to 0.25%. At 0.5% replacement level it significantly improved its 28-day strength compared to that of the 0.25% replacement level, however it was still slightly lower than that of 0.1% replacement level. At 0.75% it again showed a reduction followed by an increase in 28-day strength at 1% replacement level. However, PP biochar showed consistent results with the increase in its replacement level. The compressive strength of PP biochar blended mixes showed a reduction in its 28-day compressive strengths with the increase in its replacement levels.

Zeidabadi et al. [42] looked at investigating the effect of rice husk and bagasse biochars at 5 and 10% cement replacement levels. They observed that both the rice husk and bagasse biochars showed 5% replacement level to be the optimum replacement level that provided a small improvement in their 28-day compressive strength than the control sample. With the further increase in the replacement level, they observed a reduction in their corresponding 28-day compressive strength results. Both rice husk and bagasse biochars showed approximately a similar increase in their 28-day strength than that of the control mix. They attributed the increase in strength at 5% replacement level to the pozzolanic effect. On further increasing the biochar content, the cement's dilution effect (i.e., the reduction in the cement content) was more prominent. In another study, Gupta et al. [35] investigated the effect of wood sawdust biochar with and without CO2 saturation at 2% cement replacement level on the properties of the blended cement composites. They observed that the calcium carbonate content was higher in both the unsaturated and the CO2 saturated biochar blended composites. However, the CO2 saturated biochar showed a significant increase in its calcium carbonate content compared to both the control and the unsaturated biochar blended cement composites. They attributed this to the carbonation of the portlandite content released by the hydration reaction of OPC. The 28-day compressive strength results showed a 10% reduction in the 28-day strength of CO2 saturated biochar blended cement mortar. However, the unsaturated biochar blended mix showed 7.7% increase in its corresponding compressive strength results. The attributed the increase in the 28-day strength of the unsaturated biochar blended cement mortar to the reduction in the effective water/cement ratio due to its absorption/adsorption by the biochar particles that also contributed towards the internal curing of the cement particles.

Bioash, derived from the destructive thermal oxidation of biosolids, destroys all the organic content, including organic carbon, present in biosolids, leaving behind only the inorganic minerals. Its use in cement and concrete applications have been demonstrated recently. Garcés et al. [43] analyzed the effect of replacing ordinary Portland cement (OPC) with sewage sludge ash (SSA) derived from the incineration of sewage sludge at 800 °C in a fluidized bed reactor at a replacement level of 10, 20, and 30%. They (Garcés et al. [43]) noted that the 28-day compressive strength of the blended cement composites showed a reduction of 11.8% and 30.2% at the respective replacement levels of 10% and 30%, compared to that of the control mix. Chang et al. [44] investigated the effect of sewage sludge ash as a cement replacement material at 10, 20, and 30% of replacement levels. They (Chang et al. [44]) noticed an increase in the initial and final setting times of SSA modified cement composites that increased with the increase in the SSA content, which they attributed it to the lower fineness of SSA compared to that of the cement. The compressive strength results showed an approximate reduction of 8, 25, and 37% at the respective cement replacement levels of 10, 20, and 30%. They attributed it to the low amorphous silica content and the pozzolanic activity of the sewage sludge ash. Another study by Chen and Poon [45] noted a reduction of 9.6, 4.4, 8.8% in the respective 28-day compressive strength results of

SSA blended cement composites containing 5, 10, and 20% of SSA. Interestingly, the replacement of cement content with sewage sludge ash in their experimental work did not show any consistent correlation with its strength properties. The literature shows some contradictions on the effect of the replacement of cement with the sewage sludge ash [43–45]. Therefore, it warrants detailed investigation on the standalone material properties and its physicochemical behaviour when used as a supplementary cementitious material.

To the best of the authors' knowledge, based on the review of existing literature on the applications of different forms of treated sewage waste (raw biosolids, biochar, and bioash) [31,32,35,41–45], as cement replacement materials, there appears to be very little, or no study carried out on (i) the use of biosolids as cement replacement material (ii) use of biochar derived from dried sewage waste as a cement replacement material, and (iii) there is no existing study that investigates the comparative effect of all the three forms of treated sewage waste (biosolids, biochar, and bioash). Moreover, identifying the potential applications of biosolids/biochar/bioash in cement and concrete industry can help preserve the valuable natural resources that have to be mined continuously to meet the concrete industry's growing demand. Therefore, to address these research gaps and to look for solutions to an environmental problem associated with this waste product, a comprehensive study was undertaken in a two-staged approach. In the first stage, we looked at investigating the physical, elemental, and mineralogical changes within the material properties of the three forms (raw biosolids, biochar, and bioash) of treated sewage waste. X-ray fluorescence (XRF), X-ray diffraction (XRD), scanning electron microscopy (SEM), energy-dispersive X-ray spectroscopy (EDX), and Carbon, Hydrogen, Nitrogen, and Sulfur (CHNS) analysis were undertaken to investigate the elemental and mineralogical properties of biosolids, biochar, and bioash. In the second stage, we investigated all these three forms of treated sewage waste as cement replacement materials at 5 and 10 wt% replacement levels. To investigate the variation in the mechanical and physicochemical properties of hardened cement mortars of the blended cement composites, compressive strength, thermogravimetric analysis (TGA), XRD, and X-ray tomographic (XRT) analysis were undertaken.

2. Raw material and experimental program

2.1. Raw material

The raw materials used in this experimental program were Australian Builders GP Cement (OPC) procured from Independent cement P/L, biosolids, pyrolytic biochar from biosolids, bioash from biosolids, sand, water, and superplasticiser (MasterGlenium SKY 8379 from BASF). The biosolids used in this study were sourced from Boneo water recycling facility of South East Water Corporation in Victoria, Australia. Biosolids were produced after aerobic and anaerobic digestion, followed by dewatering (belt press) and drying (solar drying sheds) [46]. Biochar was produced by slow pyrolysis of the harvested biosolids from solar dryer sheds in a lab-scale bubbling fluidized bed reactor at 600 °C and 1000 ml min^{-1} of nitrogen flowrate with a constant heating rate of 35 °C min^{-1} and 60 min solid residence time. The detailed procedure of biosolids pyrolysis is described in our previous work [37]. To produce bioash, the organic matter content of the biosolids was destroyed by keeping it in a muffle furnace at 550 °C temperature for 12 h [47].

2.2. Particle size distribution of ordinary portland cement, biosolids, biochar and bioash

The particle size distribution of ordinary portland cement, biosolids, biochar, and bioash was obtained using laser diffraction particle size analyser "Malvern Mastersizer 3000″

2.3. Chemical properties of ordinary portland cement, biosolids, biochar and bioash

To ascertain the elemental composition and chemical phases present in various raw materials, XRF (Bruker – Massachusetts, USA), XRD (Bruker – Massachusetts, USA), and CHNS (PerkinElmer – Massachusetts, USA) analysis were undertaken. Since various methods of elemental quantification have their own limitations, multiple techniques were used to quantify all the elements present in biosolids, biochar, and bioash.

2.3.1. Quantification of elemental composition

X-ray fluorescence cannot detect elements below sodium (Na) in the periodic table. Therefore, to quantify other elements, energy-dispersive x-ray spectroscopy (EDX) and carbon, hydrogen and nitrogen (CHNS) analysis were also undertaken. For EDX analysis, powdered samples were applied onto the carbon tape affixed on top of the steel stubs. 10nm of platinum coating was applied onto the samples for better conductivity using Leica EM ACE600 Sputter Coater instrument. SEM-EDX was carried out on these samples using FEI Quanta 200 SEM equipped with Oxford XMax20 EDS Detector. EDX spectra was taken at different locations of the sample at 1000x magnification level. For CHNS analysis ~2.5mg of powdered samples were loaded into the aluminium vials and transferred into the PerkinElmer Series II CHNS analyser instrument for carbon, hydrogen, nitrogen, and sulfur analysis. Three replicates were taken for each material to identify any variation in the results. The mean value of the three replicates and its standard deviation were provided in the results.

2.3.2. X-ray diffraction

X-ray diffraction provides the minerological composition of the cementitious materials used in this experiment as these minerals are instrumental in the hydration/pozzolanic reactions when they are used as cement composites. X-ray diffraction was carried out on the dried powder samples using AXS-D4-Endeavour (Bruker) equipped with Cu-Kα radiation source and lynxeye linear strip detector. Sample preparation and equipment settings for the testing are described in Roychand et al. [6].

2.4. Recycling of biosolids, biochar, and bioash as cement replacement material

2.4.1. Mortar mix design, specimen preparation, and testing

Biosolids, biochar, and bioash were used as cement replacement materials at 5 and 10% by weight of cement. 50 mm cube cement mortar samples were prepared with a water to cement ratio of 0.4 and sand to cement ratio of 2. Three replicates were casted for each curing age to compare the performance of various replacement materials on their compressive strengths at 7 and 28 days of curing. Additional cubes were casted to carry out scanning electron microscopy and x-ray microtomography on the hardened mortar specimens at 28 days of curing. All the mortar specimens were de-molded after 24 h, cured for 7 and 28 days in accordance with AS 1012.8.1:2014 [48] and tested for compressive strength as per AS 1012.9:2014 [49]. Table 1 shows the proportion of various materials in different mortar mix designs tested.

2.5. Scanning electron microscopy of mortar specimens

Scanning electron microscopy (SEM) was undertaken on the mortar specimens, using FEI Quanta 200 ESEM at 28 days of curing to identify the morphological changes taken place within the cement microstructure with the addition of biosolids, biochar, and bioash. Small 10 × 10 × 10 mm sections were cut out of the hardened mortar samples after 28 days of curing. The sliced sections were embedded in epoxy in 25 mm diameter Teflon molds and kept for drying for 24 h at room temperature (23 ± 2 °C). The exposed surface of the epoxy embedded samples was

Table 1
Mortar mix designs.

Mix	Total Binder				Sand/Binder	Water/Binder	Superplasticizer mL/kg of Binder
	OPC	Biosolids (BS)	Biochar (BC)	Bioash (BA)			
Control (C)	100%	–	–	–	2	0.4	5
BS5	95%	5%	–	–	2	0.4	5
BC5	95%	–	5%	–	2	0.4	5
BA5	95%	–	–	5%	2	0.4	5
BS10	90%	10%	–	–	2	0.4	5
BC10	90%	–	10%	–	2	0.4	5
BC10	90%	–	–	10%	2	0.4	5

Note: BS, BC, and BA were used supplementary cementitious materials at 5% and 10% by weight of cement.

grounded with 600–1200 grit silicon carbide grinding paper and then polished using 9 μm, 3 μm and 1 μm diamond suspension. Polished samples were then mounted on a steel stub and coated with gold. The SEM images were acquired at 500x, 5000x, and 20,000x magnification levels using 30 kV accelerating voltage.

2.5.1. X-ray micro-tomography of mortar specimens

X-ray micro-tomography was used to ascertain the total porosity of the hardened cement composites as total porosity has a significant influence on the mechanical properties of the hardened concrete/mortar. X-ray micro-tomography was conducted on the mortar specimens at 28 days of curing using Bruker Skyscan 1275 X-ray micro-CT system. 25mmØ x 50 mm height mortar samples were cored out of the 50 × 50 × 50 mm mortar cube samples at 27th day of curing and dried for 24 h at 40 °C temperature. X-ray micro-tomography was performed on these cored and dried mortar cylinders at 15μm resolution at 100 kV voltage and 100 mA current using Cu Filter.

2.5.2. X-ray diffraction and thermogravimetric analysis of hardened cement paste specimens

XRD and TGA provided the mineralogical composition of the reaction products of the hardened cement pastes at various curing ages, that help in ascertaining the reasons behind the variation in the strength properties of the blended cement composites. XRD and TGA were undertaken on micronized 7- and 28-day cured hardened cement paste specimens. The cement pastes were prepared using the same mix design, excluding the sand component. Solvent exchange method described in Roychand et al. [1] was used to remove the unreacted water of hydration present in the micronized powder samples, followed by oven drying at 40 °C temperature. XRD was carried out on the dried powder samples as per the method described in Roychand et al. [6]. TGA analysis was carried out on the powder samples using PerkinElmer-STA6000 thermal analyzer with the nitrogen flow rate of 19.8 mL min^{-1}. The oven-dried powdered samples were initially heated at 40 °C for 5 min to expel any moisture caught during sample handling, followed by a heating step of 40–850 °C at the heating rate of 20 °C min^{-1}.

3. Results and discussion

3.1. Particle size distribution, elemental, mineralogical, and physical comparison of biosolids, biochar, and bioash

Table 2 provides the particle size distribution of the powder cementitious material. Table 3 presents the elemental composition of biosolids, biochar, and bioash obtained from X-ray fluorescence analysis (XRF). Since XRF cannot identify the elements having atomic number lower than sodium (Na), therefore the total percentage of the identified elements shown in Table 3 are lower than 100%.

Table 2
Particle size distribution of OPC, Biosolids, Biochar and Bioash.

Material	D_{10}	D_{25}	D_{50}	D_{75}	D_{90}
OPC	2.9 μm	6.9 μm	16.3 μm	30.1 μm	46.9 μm
Biosolids	1.8 μm	5.3 μm	14.3 μm	33.3 μm	69.3 μm
Biochar	2.2 μm	5.8 μm	13.9 μm	32.9 μm	75.1 μm
Bioash	1.4 μm	4.0 μm	12.9 μm	36.3 μm	76.6 μm

Table 3
Elemental composition of biosolids, biochar and bioash.

Elements	Percentage concentration		
	Biosolids	Biochar	Bioash
Na	0.0	0.1	0.9
Mg	0.5	0.9	1.4
Al	2.0	3.8	5.2
Si	3.3	6.1	10.3
P	1.2	2.0	2.9
S	1.0	1.3	1.5
Cl	0.3	0.3	0.4
K	0.5	0.8	2.0
Ca	5.0	8.6	14.4
Ti	0.5	0.9	1.1
Cr	0.0	0.02	0.02
Mn	0.1	0.1	0.1
Fe	5.0	6.1	8.0
Ni	0.0	0.02	0.01
Cu	0.2	0.3	0.4
Zn	0.5	0.6	0.7
Br	0.1	0.1	0.2
Rb	0.0	0.0	0.01
Sr	0.2	0.3	0.3
Zr	0.0	0.0	0.1
Sn	0.0	0.04	0.06
Mo	0.02	0.0	0.0
Ru	0.02	0.0	0.0
Ba	0.1	0.17	0.3
Pb	0.03	0.04	0.03
Total	20.57	32.59	50.33

To identify the elements lower than Na, SEM-EDX analysis was undertaken (Fig. 1). EDX spectra were collected at ten different locations on each sample to identify the remaining elements in the samples, including H and O. The EDX spectra shows the presence of C, N, and O elements present in biosolids, C and O in biochar, and only O in bioash. However, it has a limitation of identifying elements having atomic mass lower than boron (B) in the periodic table; therefore, XRD was used to identify the remaining four elements (H, Li, Be and B) and to ascertain the mineralogical composition of all the three forms of biosolids.

Since organic and unburnt carbon plays an essential role in the hydration/pozzolanic reaction of cementitious materials, CHNS analysis (Table 4) was undertaken to identify C, H, N, and S elements. XRF analysis works on a volume concentration basis and CHNS analysis on a mass concentration basis; therefore, their percentage compositions are shown separately. Table 4 below provides the percentage mass of C, H, N, and S present in biosolids, biochar, and bioash samples. Fig. 2 shows the changes occurring in the physical appearance of the biosolids after conversion into biochar and bioash.

It can be noted that by pyrolising the biosolids (earthy green colour) containing a large amount of organic compounds, there was a small

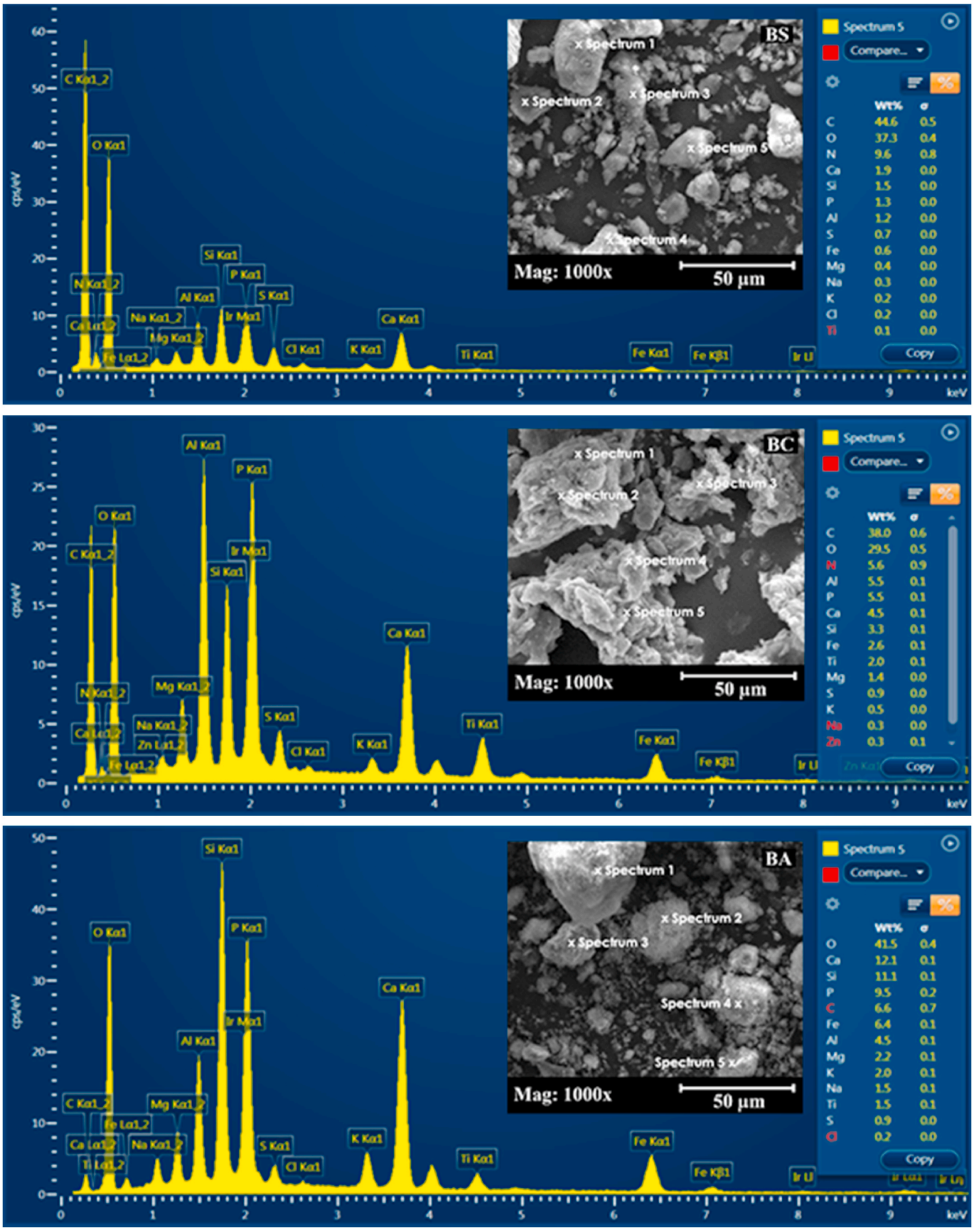

Fig. 1. SEM-EDX analysis of biosolids (BS), biochar (BC) and bioash (BA).

Table 4
Carbon, hydrogen, nitrogen, and sulfur (CHNS) percentage composition of biosolids, biochar and bioash.

Material	Carbon	Hydrogen	Nitrogen	Sulfur
Biosolids (BS)	34.7 ± 0.17	6.4 ± 0.19	6.0 ± 0.14	0.8 ± 0.18
Biochar (BC)	31.1 ± 0.18	1.3 ± 0.06	4.4 ± 0.12	1.1 ± 0.36
Bioash (BA)	0.2 ± 0.04	0.1 ± 0.05	0.1 ± 0.04	1.4 ± 0.29

reduction in C and N elements (Table 4) and a significant reduction in H (Table 4) and O (Fig. 1) in biochar. The reduction in these elements could be attributed to the thermal breakdown of organic compounds resulting in the release of chemically bound water and other volatile compounds during the pyrolysis process of biosolids. A change in the physical appearance was also noted on converting biosolids into biochar. The earthy green colour of biosolids imparted by the organic matter present in biosolids was converted to black biochar, indicating the presence of pure carbon. The XRD analysis of biosolids shows a large amount of amorphous content, as evident from the presence of an amorphous hump centered around 20° 2-theta (Fig. 3). The intensity of the amorphous hump in the XRD diffractogram of biochar decreased and shifted towards a higher 2-theta angle of ~26° 2-theta compared to that of the biosolids. Pure carbon typically shows an amorphous hump centered around 25–26° 2-theta angle [50,51]. This reinforces our observation from the physical appearance of biochar (Fig. 2) that the residual carbon left after the pyrolysis of biosolids is present as pure carbon. The presence of elemental H could be from the absorption of moisture from the atmosphere during sample handling as biochar is highly hygroscopic [52,53]. Interestingly, the CHNS analysis of biochar also showed the presence of nitrogen (Table 4). Since pure nitrogen is highly volatile and turns into gaseous form at room temperature, therefore, it is most likely present as a compound in combination with some other element. No mineral crystalline XRD peak containing nitrogen was identified in biochar, therefore it is most likely present in an amorphous form.

Bioash was produced by the destructive oxidation of biosolids by keeping it in a muffle furnace at 550 °C temperature for 12 h [47]. All the organic matter was destroyed in this process as evident from the total

Fig. 2. Photographic images showing the physical appearance of biosolids (BS) – earthy green, biochar (BC) - black and bioash (BA) - brown. (For interpretation of the references to colour in this figure legend, the reader is referred to the Web version of this article.)

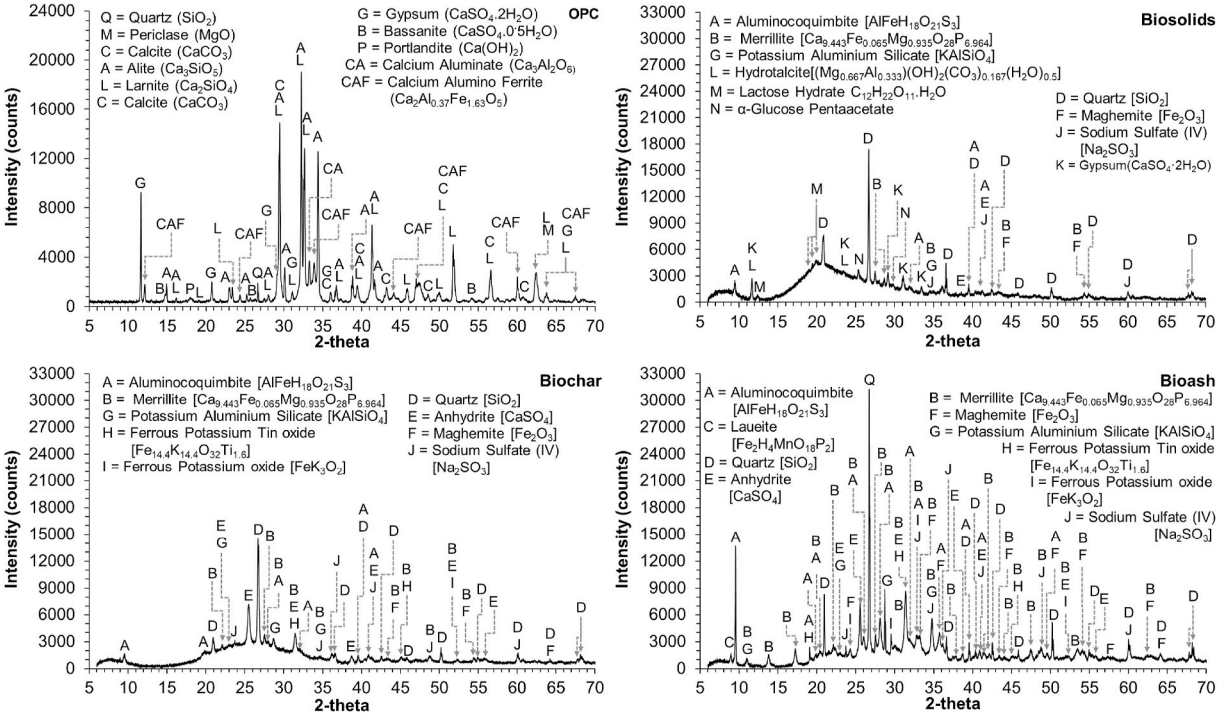

Fig. 3. X-ray diffractograms of Ordinary Portland Cement (OPC), biosolids, biochar, and bioash.

elimination of carbon, hydrogen, and nitrogen elements (Table 4), leaving behind the inorganic compounds (Fig. 3). Although all the organic compounds were eliminated, there was still a small amorphous hump visible in the X-ray diffractogram of bioash. This indicates that some inorganic compounds are present in the form of amorphous content. The earthy green colour of biosolids was converted to brown coloured bioash (Fig. 2). This was most likely because of the presence of high iron content (Table 3) that was present in the form of Maghemite mineral (Fig. 3), which is typically brown in colour [54,55]. Bioash showed an increase in the sulfur content compared to that of the raw biosolids. This is because of the oxidative destruction of organic matter present in biosolids that eliminated the carbon, hydrogen, and nitrogen elements, thereby increasing the overall proportion of sulfur present in the residual bioash.

3.2. Effect of recycling biosolids, biochar, and bioash as cement replacement material

Fig. 4 shows the compressive strength results of 7 and 28-day cured mortar samples of various mix designs. Fig. 5 presents TGA derivative curves, and Fig. 6 shows the X-ray diffractograms of hardened cement pastes at the respective curing ages. Table 5 provides an analysis of the thermogravimetric data. Fig. 7 shows the reconstructed images from the X-ray tomographic analysis.

C–S–H/C-A-S-H/AFm/Aft column shows the percentage of the chemically bound H_2O associated with this group of phases, calculated as a %age of the original mass of the micronized samples dried in an oven at 40 °C temperature.

CH_i and CC_i are the identified residual calcium hydroxide and calcite phases calculated as per the following equations:

$$CH_i = \frac{M_{H2O\ CH} * \frac{74}{18}}{M_{40}} * 100\ [\%]$$

$$CC_i = \frac{M_{CO2\ CC} * \frac{100}{44}}{M_{40}} * 100\ [\%]$$

$M_{H2O\ CH}$, and $M_{CO2\ CC}$ are the respective mass loss evident from the break down of chemically-bound H_2O present in portlandite and chemically-bound CO_2 present in calcite.

M_{40} = Mass of the original dried sample at 40 °C.

CH_{et} is the equivalent total portlandite released into the cement matrix from the hydration-reaction of C_2S and C_3S phases, calculated from the summation of actual identified portlandite (CH_i) and the one calculated by converting the identified calcite (CC_i) into the equivalent amount of portlandite as per the following equations.

3.2.1. Replacement of ordinary portland cement (OPC) with 5% biosolids

From compressive strength results (Fig. 4), it can be noted that on partially replacing OPC with 5% of biosolids, there was 74.4% and 71% reduction in the compressive strengths of BS5 at 7 and 28 days, respectively. The TGA analysis shows a considerable reduction in the chemically-bound H_2O from the C–S–H/C-A-S-H/AFm/Aft group of phases (Table 5). However, the total actual portlandite (CH_{et}) released into the cement matrix was greater than that of the control mix. In addition, the peak intensities of hatrurite and larnite phases of BS5 located at ~32.25 and ~32.66° 2 theta angles showed a reduction of 11.7% and 5.3% at 7 days and 28.3% and 28.9% at 28 days of curing, respectively (Fig. 6). This clearly indicates that there is an increase in the hydration reaction of the OPC component of BS5, when compared to that of 100% OPC mix. The XRD peak intensity of ettringite ($Ca_6Al_2(SO_4)_3(OH)_{12}{\cdot}26H_2O$) shows a small reduction and that of calcium hemicarboaluminate ($Ca_4Al_2(CO_3)_{0.5}(OH)_{13}{\cdot}5H_2O$) and calcium monocarboaluminate ($Ca_4Al_2(CO_3)(OH)_{12}{\cdot}5.5H_2O$) phases shows a small increase in BS5 than that of the control mix. The chemically bound water present in ettringite is significantly higher than that of both the hemicarboaluminate and mono-carboaluminate phases. Therefore, the reduction in the chemically-bound H_2O related to the C–S–H/C-A-S-H/Aft/AFm phases, in-spite of the increase in the hydration reaction of OPC content is most likely because of the reduction in the ettringite content of BS5, compared to that of the control mix.

The thermo-gravimetric analysis of BS5 showed a considerable increase in the calcite content at both 7 and 28days of curing, when compared to that of the OPC control mix (Table 5). Previous studies have reported the production of CO_2 [56] and some other gases [56,57] from the reaction of biosolids in alkaline conditions. The increase in the calcite content of BS5 indicates the potential release of CO_2 during the hydration reaction. The X-ray tomographic analysis (Table 6) showed a substantial increase in the total porosity of BS5 (9.91%) in comparison to that of the OPC control mix (0.79%). A considerable increase in the calcite content in addition to a substantial increase in the total porosity of BS5 indicate the production of CO_2 and possibly some other gases from the reaction of biosolids with the alkaline portlandite content. The overall TGA, XRD and X-ray tomographic analysis clearly show that the significant increase in the total porosity of BS5 is the primary reason behind the decline in its 7 and 28 days compressive-strength results in-spite of a considerable increase in its hydration reaction.

3.2.2. Replacement of ordinary portland cement with 10% biosolids

With a further increase in the replacement of biosolid to 10% in BS10, there was 99.4% and 80.3% reduction in the compressive strengths at 7 and 28 days, respectively, compared to that of the OPC control mix (Fig. 4). The TGA data showed a significant reduction in the chemically-bound H_2O from the C–S–H/C-A-S-H/AFm/Aft phases at 7days when compared to that of the OPC control mix (Table 5). This reduction was significantly higher in BS10 than what was evident in BS5, indicating the negative effect of the addition of biosolids that increased with the increase in biosolids content. The X-ray diffractogram of BS10 (Fig. 6) showed a negligible amount of identified (CH_i) portlandite followed by a noticeable increase in the peak intensities of hatrurite and larnite phases at 7 days of curing. This indicates that there

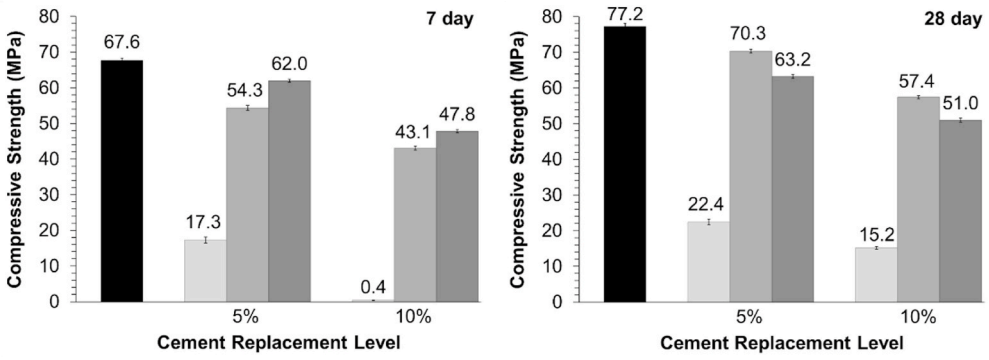

Fig. 4. Compressive strength of mortar samples.

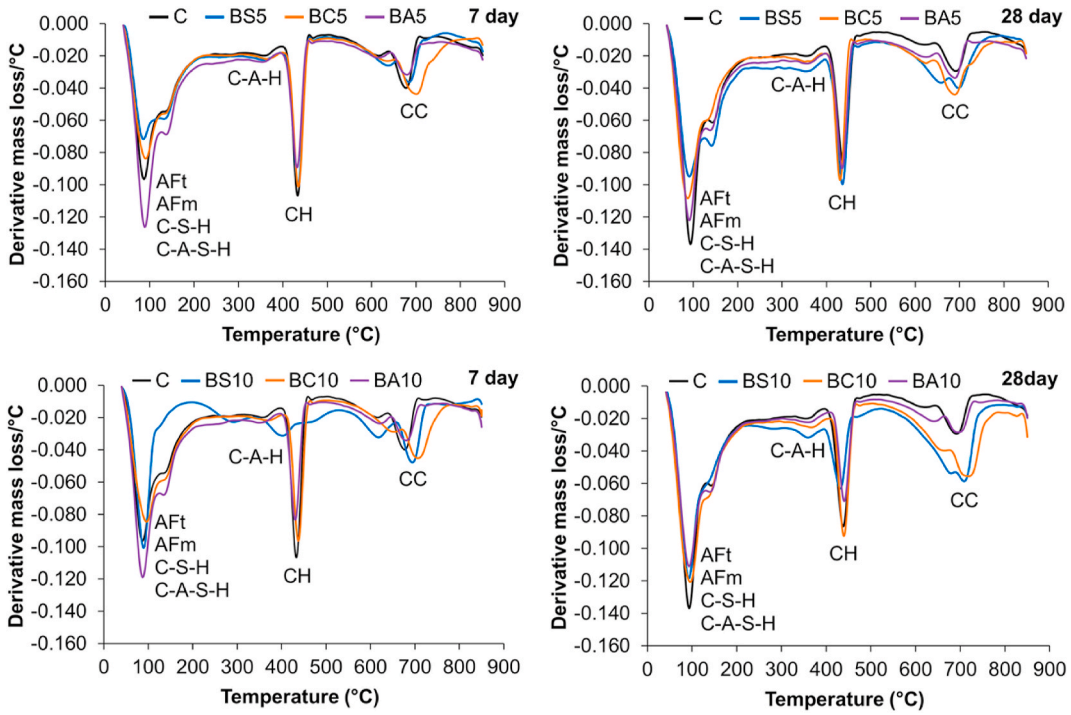

Fig. 5. Thermogravimetric derivative curves of hydrated cement composites.

was a considerable reduction in the hydration reaction of OPC present in BS5, and whatever portlandite was produced in the system, it got converted into calcite due to the possible release of CO_2 from the biosolids and portlandite reaction.

A significant amount of mass loss was identified at three TGA endothermic peaks of BS10 located at 290, 400, and 470 °C temperatures (Fig. 5). However, The XRD diffractogram of 7-day BS10 (Fig. 6) did not show any new crystalline peak that could be associated with these new complex compounds indicating that they were most likely present as an amorphous content. At 28-days, the chemically-bound H_2O from the C–S–H/C-A-S-H/AFm/Aft phases improved significantly compared to that at 7 days (BS10). However, it was still noticeably lower than that of the OPC control mix and slightly lower than that of BS5 (Table 5). The total equivalent portlandite (CH_{et}) content of BS10 was slightly higher than that of BS5; however, the hatrurite and larnite phases showed an increase in their peak intensities in-spite of the increase in biosolids content. This indicates that with the increase in the biosolids content in BS10, both the hydration reaction and the consumption of its released portlandite got negatively affected. The TGA data and the X-ray tomographic analysis of BS10 both showed a significant increase in its calcite content and total porosity, in comparison to that of BS5. This reinforces our earlier observation that the portlandite produced by the hydration of OPC, reacts with biosolids to produce CO_2, that not only increases the formation of calcite content but also raises its total porosity. The reduction in the hydration reaction of BS10 followed by a significant increase in its total porosity (16.92%) was most likely the reason behind the decline in its strength compared to that of BS5.

It is interesting to note that the addition of 10% biosolids in BS10 increases its porosity to 16.92% that is equivalent to 16.92% reduction in its density. Typically, air bubbles are introduced into concrete for various targeted benefits, such as (i) to reduce its density [58] (ii) to improve its freeze-thaw resistance (reference) (iii) to improve fire resistance (iv) to improve thermal insulation and (v) to improve acoustic properties. Therefore, the potential biosolids application in concrete could provide dual benefits viz. (i) it can help in increasing the utilisation rate of biosolids, and (ii) it can be used as an air-entraining admixture for various targeted applications. This can form part of our future study.

3.2.3. *Replacement of ordinary portland cement with 5% biochar*

When OPC was partially replaced with 5% of biochar in BC5, there was a reduction of 19.7% and 8.9% in its 7- and 28-day compressive-strength results (Fig. 4), respectively, in comparison to that of the control mix. Interestingly, it showed 213.9 and 213.8% improvement in the corresponding 7 and 28-day strengths over that of BS5, indicating significant benefits of pyrolising the biosolids. The TGA data of BC5 showed a considerable reduction in the chemically-bound H_2O from the C–S–H/C-A-S-H/AFm/Aft phases (Table 5), in comparison to that of the OPC control mix at both 7 and 28-day cured samples. However, compared to that of BS5, it showed a small improvement at 7 days and approximately similar mass loss at 28 days of curing. The XRD diffractograms of BC5 (Fig. 6) showed 8.7 and 9.1% reduction in the peak intensities of hatrurite and larnite phases (~32.25 and ~32.66° 2-theta) at 7days, and at 28days it showed a reduction of 11.7 and 8.5% in the corresponding peak intensities, in comparison to that of the OPC control mix. This signifies that there was an increase in the hydration reaction of the OPC content of BC5 at both 7 and 28 days of curing, which was also supported by the corresponding increase in its equivalent portlandite content at both the curing ages. The reduction in the C–S–H/C-A-S-H/AFm/Aft phases of BC5, in-spite of a small increase in the hydration reaction, could be attributed to the reduction in its ettringite content that showed 7 and 10.3% reduction at 7 and 28 days of curing when compared to that of the OPC control mix.

The X-ray tomographic analysis show 63% increase in the total porosity of BC5 than that of the OPC control mix (Table 6). This increase in the total porosity is most likely the reason behind the decline in its 7 and 28-day compressive-strength results compared to that of the OPC control mix. The thermo-gravimetric analysis of BC5 shows a considerable increase in the calcite content of BC5 compared to that of the control mix. However, the only source of carbon present in BC5 is pure residual carbon produced from the pyrolysis of organic compounds present in biosolids, which are non-reactive at room temperature. Previous study by Yang et al. [59] on conversion of biosolids into biochar

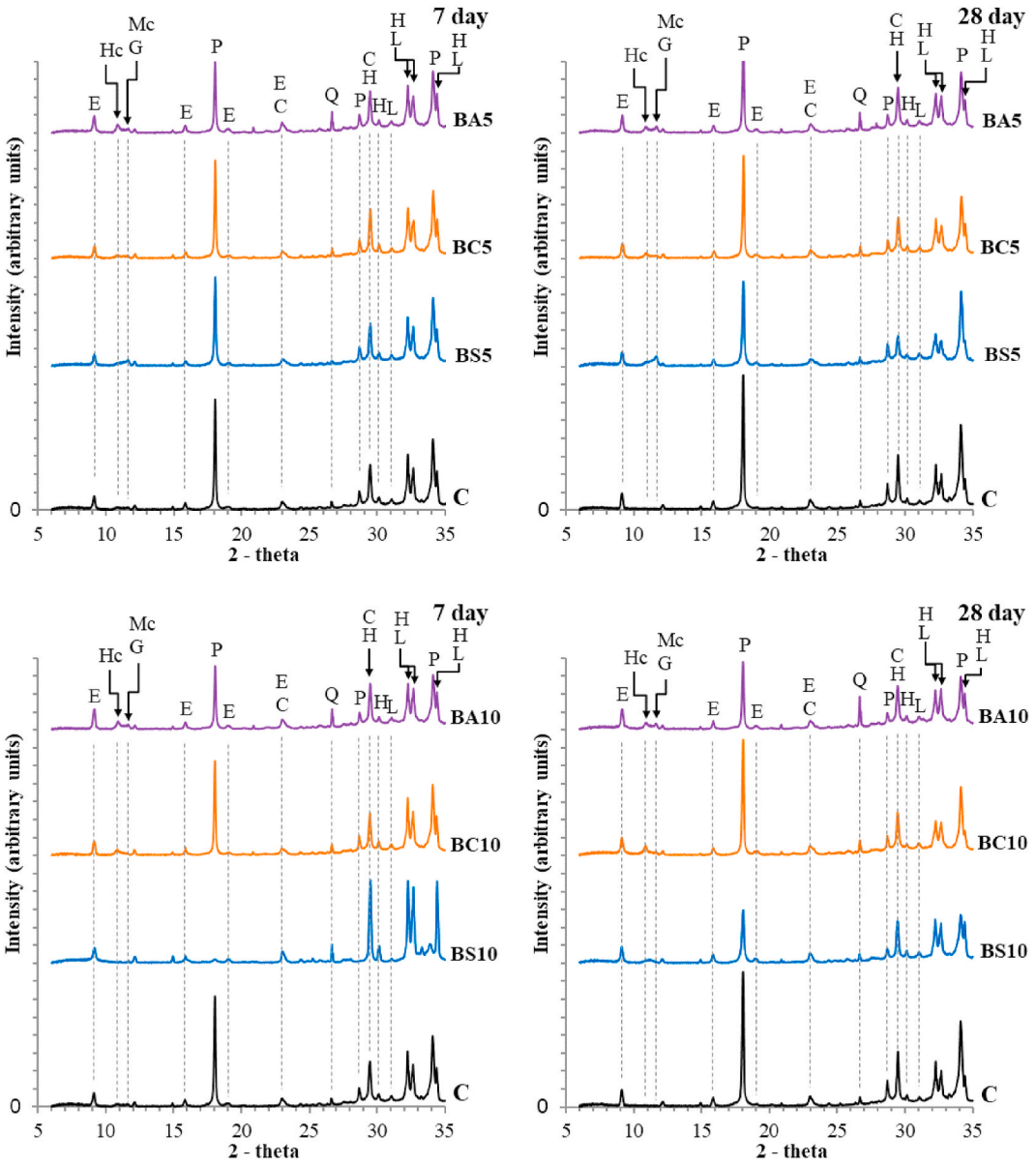

Fig. 6. XRD of hydrated cement composites.

Table 5
TGA analysis of hydrated cement composites.

Mix.	C–S–H/C-A-S-H/Aft/AFm (%)		CAH (%)		CH_i (%)		CC_i (%)		CH_{et} (%)	
	7 day	28 day	7 day	28 day	7 day	28 day	7 day	28 day	7 day	28 day
C	8.52	10.50	1.54	1.90	12.45	13.16	8.22	7.95	18.53	19.05
BS5	7.55	9.34	1.94	2.10	12.60	13.77	10.20	12.52	20.15	23.03
BC5	7.88	9.28	1.84	2.00	11.69	10.89	12.55	12.94	20.98	22.27
BA5	9.82	9.88	1.75	1.92	10.79	11.11	7.28	7.66	15.21	15.55
BS10	4.93	9.14	–	2.32	[a]	10.61	11.86	17.21	8.78	23.35
BC10	7.90	10.26	1.86	2.19	10.70	11.32	12.77	16.86	20.15	23.80
BA10	9.43	9.52	1.73	2.04	9.64	9.07	7.92	8.20	15.50	15.14

[a] Negligibly small amount of portlandite as identified in the X-ray diffractogram.

found that is it is highly porous in nature, that can trap atmospheric CO_2 in its pore structure. This trapped CO_2 is most likely responsible for the carbonation of the residual portlandite, resulting in the increase in calcite content in comparison to that of the OPC control mix.

3.2.4. Replacement of ordinary portland cement with 10% biochar

With a further increase in the replacement of biochar to 10% in BC10, there was 36.2% and 25.6% reduction in the compressive strength at 7 and 28days, respectively, compared to that of the 100% OPC control

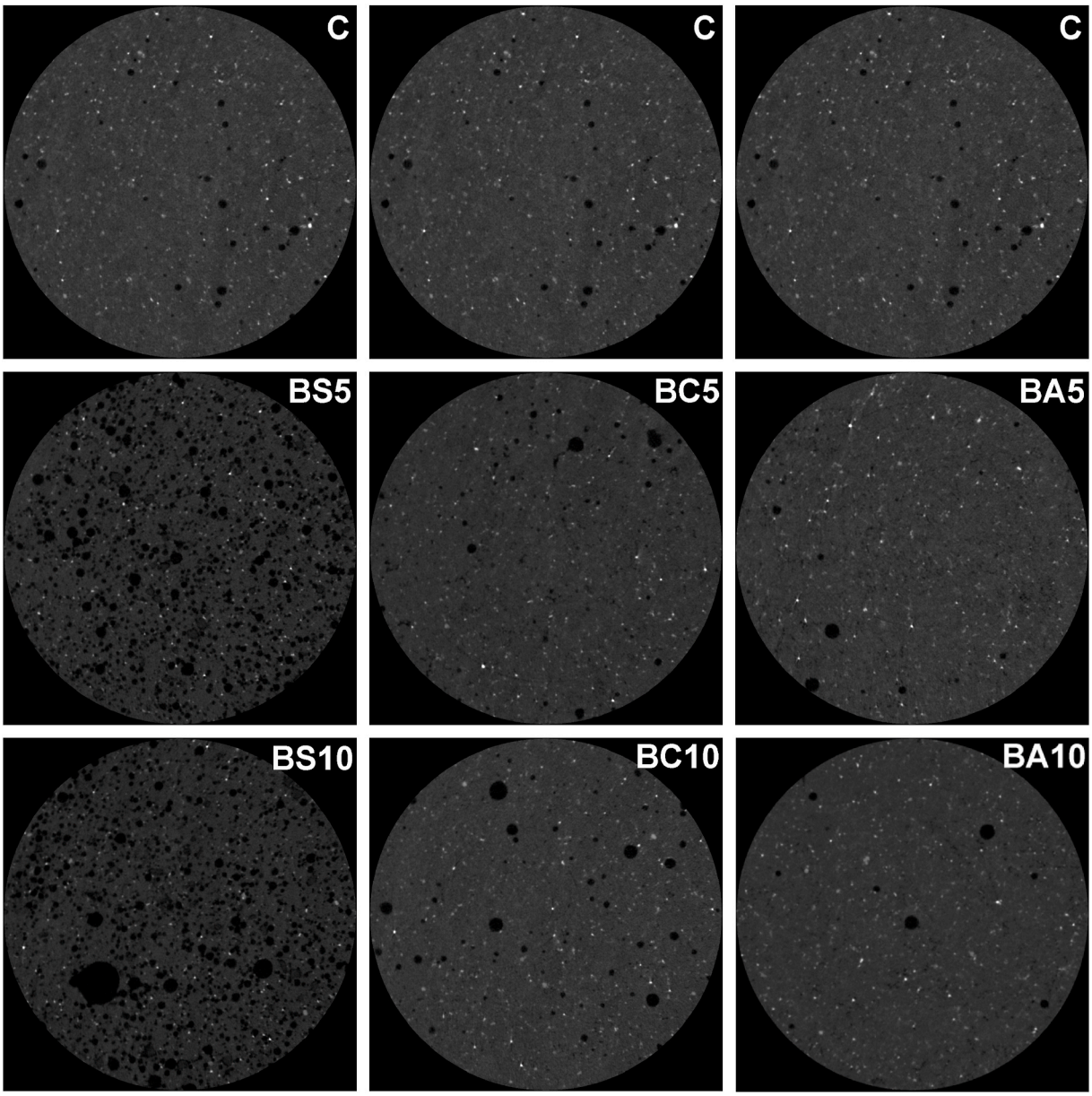

Fig. 7. X-ray tomography reconstructed images of hardened mortar samples.

Table 6
Total porosity obtained from micro computed tomographic analysis of hardened mortar samples.

	C	BS5	BC5	BA5	BS10	BC10	BA10
Total Porosity (%)	0.79	9.91	1.29	0.72	16.92	2.21	0.76

mix (Fig. 4). This reduction in strength was considerably higher than what was observed in BC5. The TGA data of BC10 showed similar mass-loss of the chemically-bound H_2O from the C–S–H/C-A-S-H/Aft/AFm phases at 7-day; however, at 28-day, it showed a considerable increase in comparison to that BC5. The hatrurite and larnite phases of 7-day BC10 showed 14 and 14.5% increase in their XRD peak intensities, indicating a reduction in the hydration reaction compared to that of BC5, which was also evident in the reduction in its equivalent total portlandite content (CH_{et}). The ettringite peak intensity of BC10 showed an increase of 9.8% compared to that of BC5. Even hemi-carboaluminate phase of BC10 showed an increase in its peak intensity compared to that of BC5. Therefore, BC10 having similar mass loss at 7 days as that of BC5, in-spite of the reduction in hydration reaction of BC10 most likely because of the increase in its ettringite and hemi-carboaluminate contents.

At 28 days hatrurite and larnite peak intensities showed a reduction of 6 and 0.4%, compared to that of BC5, the average of which is lower than what ideally should have reduced with the 5% reduction in the OPC content of BC10. This indicates there was a small reduction in the hydration reaction of OPC component of BC10 due to the presence of 10% biochar. The peak intensities of ettringite and hemi-carboaluminate increased further at 28 days, which is most likely the reason behind the increase in mass-loss linked to the C–S–H/C-A-S-H/AFm/Aft phases. Therefore, The X-ray tomographic analysis show 180% increase in the total porosity of BC5 in comparison to that of the control mix and 71% higher than that of BC5. Therefore, the reduction in hydration reaction and the increase in total porosity of BC10 are most likely the reasons behind the reduction in its 7 and 28-day strengths compared to both BC5 and the control mix. The increase in the calcite content and the total porosity of BC10 than that of BC5 is most likely because of the increase

in biochar content that can entrap more air due to its porous structure. The density of air being very low, gets displaced by the water of hydration present in the mortar mix. The CO_2 present in the entrapped air carbonates the portlandite released into the cement matrix, resulting in the increase in calcite content and some unreacted air gets trapped during the hardening process thereby increasing its total porosity.

Previous studies on the effect of the addition of biochar as a cement replacement material show that they absorb a proportion of the mixing water because of their high surface area, pore volume, and water absorption capacity, which results in a reduction in the total water/cement ratio in the biochar replaced cement [60,61]. This absorbed water also helps in the internal curing of the cement matrix. Therefore, the reduction in the effective water/cement ratio and internal curing provided by the water stored in the capillary pores of biochar helps in recovering the strength loss to some extent due to the reduction in the cement content in the blended mix designs [61–63].

3.2.5. Replacement of ordinary portland cement with 5% bioash

On partly replacing OPC with 5% bioash in BA5, there was 8.3% and 18.1% reduction in the corresponding 7 and 28 day compressive strength compared to that of the 100% OPC mix. However, compared to that of BC5, BA5 showed 14.2% increase at 7 days and 10.1% reduction at 28days. The TGA data showed a considerable increase in the chemically-bound water from the C–S–H/C-A-S-H/AFm/Aft phases, compared to that of BC5, at both 7 and 28days of curing. The XRD diffractograms show a reduction in the peak intensities of hartrurite and larnite phases at 7 days, however, at 28 days the intensities of these peaks were higher than that of BC5. This indicates that the hydration reaction of the OPC component of BA5 accelerated at early ages (uptil 7 days), compared to that of BC5 due to the presence of bioash. However, it showed a slowed down reaction past 7 days as evident in the reduction in hatrurite and larnite phases at 28 days. The ettringite, hemi-carboaluminate and mono-carboaluminate phases also show an increase in the intensities of the XRD peaks in comparison to that of BC5. Therefore, the increase in the 7 days strength of BA5 in addition to a considerable increase in the mass-loss from the C–S–H/C-A-S-H/Aft/AFm phases, is most likely because of the increase in hydration reaction and the corresponding increase in ettringite, mono-carboaluminate and hemi-carboaluminate phases.

Beyond 7 days, there was no noticeable change in the ettringite content, but a small conversion of hemi-carboaluminate to the mono-carboaluminate phase was observed. In addition, the hydration reaction of the OPC component of BA5 also slowed down. However, the X-ray tomographic data showed an improvement in the total porosity of BA5 compared to that of the BC5. The increase in the chemically bound water of BA5 compared to that of BC5 at 28 days is most likely because of the increase in ettringite, mono-carboaluminate and hemi-carboaluminate phases, and the reduction in its 28 day strength is most likely because of the reduction in the hydration reaction of its (BA5) OPC component. The reduction in the total porosity of BA5 in comparison to that of BC5 must have provided a positive contribution; however, the reduction in its (BA5) hydration reaction may have been more dominant in reducing its 28-day strength. Interestingly, BA5 showed a substantial reduction in its 7 and 28-day calcite content in comparison to that of both BS5 and BC5, indicating that bioash does not provide any contributing factor that carbonates the residual portlandite content as was observed in BS5 and BC5.

3.2.6. Replacement of ordinary portland cement with 10% bioash

With a further increase in the replacement of bioash to 10% in BA10, there was 29.3% and 33.9% reduction in compressive strength at 7 and 28days, respectively, compared to that of the control mix. The thermo-gravimetric data of BA10 showed a noticeable increase in the chemically-bound H_2O from the C–S–H/C-A-S-H/AFm/Aft phases at 7days; however, at 28 days it showed a noticeable reduction in the corresponding group of phases, in comparison to that of both the control mix and BC10. The XRD diffractograms show a reduction in the peak intensities of hartrurite and larnite phases at 7 days; however, at 28 days, the intensities of these peaks were higher than that of BC10. This indicates that the hydration reaction of the OPC component of BA10 accelerated at early ages (until 7 days), compared to that of BC10 due to the presence of bioash. However, it showed a slowed down reaction past 7 days as evident in the reduction in hatrurite and larnite phases at 28 days. A similar trend was observed in BA5 compared to that of BC5. The ettringite, hemi-carboaluminate and mono-carboaluminate phases also showed an increase in their peak intensities compared to that of BC10. Therefore, the increase in the 7 days strength of BA5 in addition to a considerable increase in the mass-loss from the C–S–H/C-A-S-H/AFm/Aft phases. This is most likely because of the increase in hydration reaction and the corresponding increase in ettringite, mono-carboaluminate and hemi-carboaluminate phases.

Beyond 7 days, there was no noticeable change in the ettringite content, but a small conversion of hemi-carboaluminate to the mono-carboaluminate phases was observed. In addition, the hydration reaction of the OPC component of BA10 also slowed down from 7 to 28 days of curing. However, the X-ray tomographic data showed a considerable improvement in the total porosity of BA10 in comparison to that of the BC10. The decrease in the 28-day strength of BA10 in comparison to that of BC10 is most likely because of the reduction in its (BA10) hydration reaction that was evident. The reduction in its total porosity does not appear to have been dominant enough compared to the reduction in its hydration reaction, that resulted in its strength reduction at 28 days compared to that of BC10. A similar trend in a significant reduction in the calcite content of BA10 compared to that of BS10 and BC10 was observed as BC5 showed in comparison to that of BS5 and BC5. This reinforces our earlier observations that both biosolids and biochar provided the contributing factors that resulted in the partial carbonation of portlandite contents of BS5 and BC5.

Similar findings on the increase in hydraulic/pozzolanic activity using sewage sludge ash was reported by Ref. [64]. However, the reduction in the OPC content is more prominent in reflecting the reduction in its 7 and 28-day compressive strengths than the increase in hydraulic/pozzolanic activity. Similar findings were reported by Refs. [65,66].

4. Conclusions (C) and recommendations for future work (R)

C1 Earthy green colour of biosolids imparted by the organic compounds present in it was converted to black in colour after pyrolysis, due to destruction of organic compounds leaving behind amorphous carbon-rich biochar. However, the thermal oxidative destruction of biosolids not only destroyed its organic content including the organic carbon, leaving behind brown coloured bioash powder, which gets its colour from the presence of high amount of ferrous oxide content.

C2 Biosolids blended cement composites produce large amount of CO_2 gas due to the reaction of alkaline portlandite with the organic content present in the biosolids, leading to a significant increase in its total porosity, which increases with the increase in the biosolids content. This significant increase in the total porosity of the biosolids blended cement composites brings about a substantial reduction in its 7 and 28-day compressive strength results.

C3 Among all the three forms of biosolids (i.e., raw, pyrolyzed, and ashed), biochar provides the best performance as a cement replacement material, that provides the lowest reduction in its compressive strength results.

R1 The increase in total porosity with the addition of biosolids could help in achieving various targeted benefits, such as the reduction in concrete density, improvement in its freeze-thaw resistance, fire resistance, thermal insulation, and acoustic properties. Therefore, it can be used as an alternative to air entraining admixtures that are currently being used, that forms part of a recommendation for the future research.

R2 Previous research on biochar [67] has shown that it provides

additional benefits like humidity control, low thermal conductivity, insulation, noise protections, binding of volatile organic compounds, protection against electromagnetic radiation, anti-bacterial/fungicidal, and air cleaning properties. These properties can be investigated as part of the recommendations for future work on the biochar derived from biosolids.

R3 Since durability properties are key before any new product can be accepted by the construction industry, long term durability studies are required to be carry out on cement composites containing biosolids, biochar and bioash, that form part of the recommendations for the future work.

R4 Presence of chloride [68] and phosphorous [69] contents can have negative effect on the reinforced concrete applications if they are present in large quantities. Their concentration should be identified in the raw materials, and if present in large quantities, their individual effects should be studied in detail.

CRediT authorship contribution statement

Rajeev Roychand: Conceptualization, Methodology, Investigation, Data curation, Formal analysis, Visualization, Writing - review & editing. **Savankumar Patel:** Visualization, Writing - review & editing. **Pobitra Halder:** Visualization, Writing - review & editing. **Sazal Kundu:** Visualization, Writing - review & editing. **James Hampton:** Visualization, Writing - review & editing. **David Bergmann:** Visualization, Writing - review & editing. **Aravind Surapaneni:** Visualization, Writing - review & editing. **Kalpit Shah:** Conceptualization, Visualization, Writing - review & editing. **Biplob Kumar Pramanik:** Conceptualization, Visualization, Writing - review & editing.

Declaration of competing interest

The authors declare that they have no known competing financial interests or personal relationships that could have appeared to influence the work reported in this paper.

Acknowledgements

The authors would like to thank South East Water Corporation (Victoria, Australia) for funding this research. The authors fully acknowledge the technical support provided by the Civil, Rheology and material characterization, Microscopy & microanalysis, and the X-ray diffraction facilities at RMIT University.

References

[1] R. Roychand, S. De Silva, D. Law, S. Setunge, High volume fly ash cement composite modified with nano silica, hydrated lime and set accelerator, Mater. Struct. 49 (5) (2016) 1997–2008.
[2] R. Roychand, S. De Silva, D. Law, Setunge, and Materials, *Micro and nano engineered high volume ultrafine fly ash cement composite with and without additives*, Int. J. Concrete Struct. Mater. 10 (1) (2016) 113–124.
[3] R. Roychand, S. De Silva, S. Setunge, D. Law, A Quantitative Study on the Effect of Nano SiO2, Nano Al2O3 and Nano CaCO3 on the Physicochemical Properties of Very High Volume Fly Ash Cement Composite, European Journal of Environmental and Civil Engineering, 2017, pp. 1–16.
[4] R. Roychand, S. De Silva, S. Setunge, Nanosilica modified high-volume fly ash and slag cement composite: environmentally friendly alternative to OPC, J. Mater. Civ. Eng. 30 (4) (2018), 04018043.
[5] R. Roychand, B.K. Pramanik, G. Zhang, S. Setunge, Recycling steel slag from municipal wastewater treatment plants into concrete applications–A step towards circular economy, Resour. Conserv. Recycl. 152 (2020) 104533.
[6] R. Roychand, J. Li, S. De Silva, M. Saberian, D. Law, B.K. Pramanik, Development of zero cement composite for the protection of concrete sewage pipes from corrosion and fatbergs, Resour. Conserv. Recycl. 164 (2021) 105166.
[7] M. Saberian, L. Shi, A. Sidiq, J. Li, S. Setunge, C.-Q. Li, Recycled concrete aggregate mixed with crumb rubber under elevated temperature, Construct. Build. Mater. 222 (2019) 119–129.
[8] M. Saberian, J. Li, Investigation of the mechanical properties and carbonation of construction and demolition materials together with rubber, J. Clean. Prod. 202 (2018) 553–560.
[9] S. Ghorbani, S. Sharifi, S. Ghorbani, V.W. Tam, J. De Brito, R. Kurda, Effect of crushed concrete waste's maximum size as partial replacement of natural coarse aggregate on the mechanical and durability properties of concrete, Resour. Conserv. Recycl. 149 (2019) 664–673.
[10] W.F. Santos, M. Quattrone, V.M. John, S.C. Angulo, Roughness, wettability and water absorption of water repellent treated recycled aggregates, Construct. Build. Mater. 146 (2017) 502–513.
[11] M. Saberian, J. Li, S.T.A.M. Perera, G. Ren, R. Roychand, H. Tokhi, An experimental study on the shear behaviour of recycled concrete aggregate incorporating recycled tyre waste, Construct. Build. Mater. 264 (2020) 120266.
[12] M. Saberian, J. Li, M. Boroujeni, D. Law, C.-Q. Li, Application of demolition wastes mixed with crushed glass and crumb rubber in pavement base/subbase, Resour. Conserv. Recycl. 156 (2020) 104722.
[13] E.-S. Abd-Elaal, S. Araby, J.E. Mills, O. Youssf, R. Roychand, X. Ma, Y. Zhuge, R. J. Gravina, Novel approach to improve crumb rubber concrete strength using thermal treatment, Construct. Build. Mater. 229 (2019) 116901.
[14] O. Youssf, R. Hassanli, J.E. Mills, W. Skinner, X. Ma, Y. Zhuge, R. Roychand, R. Gravina, Influence of mixing procedures, rubber treatment, and fibre additives on rubcrete performance, J. Compos. Sci. 3 (2) (2019) 41.
[15] R. Roychand, R.J. Gravina, Y. Zhuge, X. Ma, O. Youssf, J.E. Mills, A comprehensive review on the mechanical properties of waste tire rubber concrete, Construct. Build. Mater. 237 (2020) 117651.
[16] O. Youssf, J.E. Mills, T. Benn, Y. Zhuge, X. Ma, R. Roychand, R. Gravina, Development of crumb rubber concrete for practical application in the residential construction sector–design and processing, Construct. Build. Mater. 260 (2020) 119813.
[17] M. Saberian, J. Li, D. Cameron, Effect of crushed glass on behavior of crushed recycled pavement materials together with crumb rubber for making a clean green base and subbase, J. Mater. Civ. Eng. 31 (7) (2019), 04019108.
[18] L.M. Sarmiento, K.A. Clavier, J.M. Paris, C.C. Ferraro, T.G. Townsend, Critical examination of recycled municipal solid waste incineration ash as a mineral source for portland cement manufacture–A case study, Resour. Conserv. Recycl. 148 (2019) 1–10.
[19] E.T. Bueno, J.M. Paris, K.A. Clavier, C. Spreadbury, C.C. Ferraro, T.G. Townsend, A review of ground waste glass as a supplementary cementitious material: a focus on alkali-silica reaction, J. Clean. Prod. 257 (2020) 120180.
[20] S.H. Joo, F.D. Monaco, E. Antmann, P. Chorath, Sustainable approaches for minimizing biosolids production and maximizing reuse options in sludge management: a review, J. Environ. Manag. 158 (2015) 133–145.
[21] W. Rulkens, Sewage sludge as a biomass resource for the production of energy: overview and assessment of the various options, Energy Fuel. 22 (1) (2007) 9–15.
[22] A.a.N.Z.B. Partnership, Australian Biosolid Statistics, 2019, Australia and New Zealand Biosolids Partnership, 2019.
[23] M.M. Roy, A. Dutta, K. Corscadden, P. Havard, L. Dickie, Review of biosolids management options and co-incineration of a biosolid-derived fuel, Waste Manag. 31 (11) (2011) 2228–2235.
[24] R. Gibbs, C. Hu, G. Ho, I. Unkovich, Regrowth of faecal coliforms and salmonellae in stored biosolids and soil amended with biosolids, Water Sci. Technol. 35 (11–12) (1997) 269–275.
[25] M. Rogers, S.R. Smith, Ecological impact of application of wastewater biosolids to agricultural soil, Water Environ. J. 21 (1) (2007) 34–40.
[26] S. Mattigod, A. Page, Assessment of metal pollution in soils, in: I. Thornton (Ed.), Applied Environmental Geochemistry, Academic Press, 1983.
[27] E.Z. Harrison, M.B. McBride, D.R. Bouldin, Land application of sewage sludges: an appraisal of the US regulations, Int. J. Environ. Pollut. 11 (1) (1999) 1–36.
[28] R. Roychand, B.K. Pramanik, Identification of micro-plastics in Australian road dust, J. Environ. Chem. Eng. 8 (1) (2020) 103647.
[29] PFAS NEMP 2.0 Environment Protection Authority Victoria. Available from: https://www.epa.vic.gov.au/for-community/environmental-information/pfas/pfas-nemp-2-0.
[30] T.L. Coggan, D. Moodie, A. Kolobaric, D. Szabo, J. Shimeta, N.D. Crosbie, E. Lee, M. Fernandes, B.O. Clarke, An investigation into per-and polyfluoroalkyl substances (PFAS) in nineteen Australian wastewater treatment plants (WWTPs), Heliyon 5 (8) (2019), e02316.
[31] A. Ukwatta, A. Mohajerani, S. Setunge, N. Eshtiaghi, Possible use of biosolids in fired-clay bricks, Construct. Build. Mater. 91 (2015) 86–93.
[32] W.R. Mozo-Moreno, A. Gómez, Biosolids and biosolid ashes as input for producing brick-like construction materials, Tecciencia 11 (21) (2016) 45–51.
[33] A. Callegari, A.G. Capodaglio, Properties and beneficial uses of (bio) chars, with special attention to products from sewage sludge pyrolysis, Resources 7 (1) (2018) 20.
[34] S. Praneeth, L. Saavedra, M. Zeng, B.K. Dubey, A.K. Sarmah, Biochar admixtured lightweight, porous and tougher cement mortars: mechanical, durability and micro computed tomography analysis, Sci. Total Environ. 750 (2020) 142327.
[35] S. Gupta, H.W. Kua, C.Y. Low, Use of biochar as carbon sequestering additive in cement mortar, Cement Concr. Compos. 87 (2018) 110–129.
[36] R. Liu, H. Xiao, S. Guan, J. Zhang, D. Yao, Technology and method for applying biochar in building materials to evidently improve the carbon capture ability, J. Clean. Prod. 273 (2020) 123154.
[37] S. Patel, S. Kundu, P. Halder, G. Veluswamy, B. Pramanik, J. Paz-Ferreiro, A. Surapaneni, K. Shah, Slow pyrolysis of biosolids in a bubbling fluidised bed reactor using biochar, activated char and lime, J. Anal. Appl. Pyrol. 144 (2019) 104697.
[38] A. Capodaglio, A. Callegari, D. Dondi, Properties and beneficial uses of biochar from sewage sludge pyrolysis, in: 5th International Conference on Sustainable Solid Waste Management, 2017.

[39] P.L. Ngo, B.K. Pramanik, K. Shah, R. Roychand, Pathway, classification and removal efficiency of microplastics in wastewater treatment plants, Environ. Pollut. 255 (2019) 113326.
[40] B.K. Pramanik, R. Roychand, S. Monira, M. Bhuiyan, V. Jegatheesan, Fate of road-dust associated microplastics and per-and polyfluorinated substances in stormwater, Process Saf. Environ. Protect. 144 (2020) 236–241.
[41] A. Akhtar, A.K. Sarmah, Novel biochar-concrete composites: manufacturing, characterization and evaluation of the mechanical properties, Sci. Total Environ. 616 (2018) 408–416.
[42] Z.A. Zeidabadi, S. Bakhtiari, H. Abbaslou, A.R. Ghanizadeh, Synthesis, characterization and evaluation of biochar from agricultural waste biomass for use in building materials, Construct. Build. Mater. 181 (2018) 301–308.
[43] P. Garcés, M.P. Carrión, E. García-Alcocel, J. Payá, J. Monzó, M. Borrachero, Mechanical and physical properties of cement blended with sewage sludge ash, Waste Manag. 28 (12) (2008) 2495–2502.
[44] F. Chang, J. Lin, C. Tsai, K. Wang, Study on cement mortar and concrete made with sewage sludge ash, Water Sci. Technol. 62 (7) (2010) 1689–1693.
[45] Z. Chen, C.S. Poon, Comparative studies on the effects of sewage sludge ash and fly ash on cement hydration and properties of cement mortars, Construct. Build. Mater. 154 (2017) 791–803.
[46] R. Irwin, A. Surapaneni, D. Smith, J. Schmidt, H. Rigby, S. Smith, Verification of an alternative sludge treatment process for pathogen reduction at two wastewater treatment plants in Victoria, Australia, J. Water Health 15 (4) (2017) 626–637.
[47] M.J. Bentley, R.S. Summers, Ash pretreatment of pine and biosolids produces biochars with enhanced capacity for organic micropollutant removal from surface water, wastewater, and stormwater, Environ. Sci.: Water Resear. Technol. 6 (3) (2020) 635–644.
[48] AS 1012.8.1, Methods of Testing Concrete - Method for Making and Curing Concrete - Compression and Indirect Tensile Test Specimens, in: GPO Box, vol. 476, Standards Australia Ltd, Sydney, NSW 2001, 2014. Australia www.standards.org.au.
[49] AS 1012.9, Compressive Strength Tests - Concrete, Mortar and Grout Specimens, Standards Australia Ltd, Sydney, NSW 2001, 2014. Australia, www.standards.org.au.
[50] A. Sharma, T. Kyotani, A. Tomita, Comparison of structural parameters of PF carbon from XRD and HRTEM techniques, Carbon 38 (14) (2000) 1977–1984.
[51] E. Antolini, F. Cardellini, Formation of carbon supported PtRu alloys: an XRD analysis, J. Alloys Compd. 315 (1–2) (2001) 118–122.
[52] S. Sohi, J. Gaunt, J. Atwood, Biochar in Growing Media: Biochar in Growing Media: A Sustainability and Feasibility Assessment A Sustainability and Feasibility Assessment, 2013.
[53] J.G. Shepherd, S.P. Sohi, K.V. Heal, Optimising the recovery and re-use of phosphorus from wastewater effluent for sustainable fertiliser development, Water Res. 94 (2016) 155–165.
[54] M.A. Legodi, D. de Waal, The preparation of magnetite, goethite, hematite and maghemite of pigment quality from mill scale iron waste, Dyes Pigments 74 (1) (2007) 161–168.
[55] I.A. Ike, M. Duke, Synthetic magnetite, maghemite, and haematite activation of persulphate for orange G degradation, J. Contam. Hydrol. 215 (2018) 73–85.
[56] A.A. Khurram, Effect of various amendments on the solids properties and gas production of biosolids, Int. J. Therm. Environ. Eng. 4 (1) (2012) 67–72.
[57] M.J. Girovich, Biosolids Treatment and Management: Processes for Beneficial Use, crc Press, 1996.
[58] N. Narayanan, K. Ramamurthy, Structure and properties of aerated concrete: a review, Cement Concr. Compos. 22 (5) (2000) 321–329.
[59] Y. Yang, B. Meehan, K. Shah, A. Surapaneni, J. Hughes, L. Fouché, J. Paz-Ferreiro, Physicochemical properties of biochars produced from biosolids in Victoria, Australia, Int. J. Environ. Res. Publ. Health 15 (7) (2018) 1459.
[60] S. Gupta, H.W. Kua, H.J. Koh, Application of biochar from food and wood waste as green admixture for cement mortar, Sci. Total Environ. 619 (2018) 419–435.
[61] S. Gupta, H.W. Kua, Effect of water entrainment by pre-soaked biochar particles on strength and permeability of cement mortar, Construct. Build. Mater. 159 (2018) 107–125.
[62] W.C. Choi, H.D. Yun, J.Y. Lee, Mechanical properties of mortar containing bio-char from pyrolysis, J. Korea Inst. Struct. Maintenance Inspect. 16 (3) (2012) 67–74.
[63] A. Dixit, S. Gupta, S. Dai Pang, H.W. Kua, Waste Valorisation using biochar for cement replacement and internal curing in ultra-high performance concrete, J. Clean. Prod. 238 (2019) 117876.
[64] M. Oliva, F. Vargas, M. Lopez, Designing the incineration process for improving the cementitious performance of sewage sludge ash in Portland and blended cement systems, J. Clean. Prod. 223 (2019) 1029–1041.
[65] T.K. David, S.K. Nair, Compressive strength of concrete with sewage sludge ash (SSA), IOP Conf. Ser. Mater. Sci. Eng. 371 (1) (2018).
[66] P. Khawal, G. Sangwai, Sewage sludge ash as a partial replacement of cement in concrete, in: Techno-Societal 2018, Springer, 2020, pp. 543–550.
[67] H. Schmidt, The use of biochar as building material, Biochar J. (2014).
[68] B.H. Oh, S.Y. Jang, Y. Shin, Experimental investigation of the threshold chloride concentration for corrosion initiation in reinforced concrete structures, Mag. Concr. Res. 55 (2) (2003) 117–124.
[69] J. Hu, Comparison between the effects of superfine steel slag and superfine phosphorus slag on the long-term performances and durability of concrete, J. Therm. Anal. Calorim. 128 (3) (2017) 1251–1263.